Journal of Alloys and Compounds 488 (2009) 246–249

Contents lists available at ScienceDirect

Journal of Alloys and Compounds

journal homepage: www.elsevier.com/locate/jallcom

Research of phase transformation on Fe–8.7Al–28.3Mn–1C–5.5Cr alloy

Chiung-Fang Huang[a,b], Keng-Liang Ou[c,d,**], Chin-Sung Chen[e,f], Chau-Hsiang Wang[g,h,*]

[a] School of Dentistry, College of Oral Medicine, Taipei Medical University, Taipei 110, Taiwan
[b] Department of Dentistry, Taipei Medical University Hospital, Taipei 110, Taiwan
[c] Research Center for Biomedical Implants and Microsurgery Devices, Taipei Medical University, Taipei 110, Taiwan
[d] Graduate Institute of Biomedical Materials and Engineering, Taipei Medical University, Taipei 110, Taiwan
[e] Department of Dentistry, Cathay General Hospital, Taipei 110, Taiwan
[f] Department of Dentistry, Cathay General Hospital, Sijhih, Taipei 110, Taiwan
[g] School of Dentistry, College of Dental Medicine, Kaohsiung Medical University, Kaohsiung, Taiwan
[h] Department of Dentistry, Kaohsiung Medical University Hospital, Taipei 110, Taiwan

ARTICLE INFO

Article history:
Received 8 March 2009
Received in revised form 20 August 2009
Accepted 21 August 2009
Available online 27 August 2009

Keywords:
Fe–Al–Mn–C–Cr alloy
Chromium carbide
Phase transformation
Electron microscopy
Heat treatment

ABSTRACT

This investigation elucidates the phase transformations of the Fe–8.7Al–28.3Mn–1C–5.5Cr alloy using optical microscopy (OM), scanning electron microscopy (SEM), transmission electron microscopy (TEM) and energy-dispersive X-ray spectrometer (EDS). As the alloy was solution heat treated and then quenched, a $(\gamma + Cr_7C_3) \rightarrow \gamma \rightarrow (\gamma + (\alpha + B2 + DO_3))$ phase transition was observed within the austenite matrix. During aging treatment at 400–800 °C, a $\gamma \rightarrow (\gamma + \kappa) \rightarrow (\gamma + Cr_{23}C_6) \rightarrow (\gamma + Cr_{23}C_6 + Cr_7C_3) \rightarrow (\gamma + Cr_7C_3)$ phase transition was observed within the austenite matrix. When the alloy underwent aging treatment between 400 and 500 °C, some $(Fe, Mn)_3AlC_x$ κ-phase carbides formed in the matrix and grain boundaries. A $\gamma \rightarrow (DO_3 + Cr_{23}C_6) \rightarrow (DO_3 + Cr_{23}C_6 + Cr_7C_3) \rightarrow (DO_3 + Cr_7C_3)$ phase transition was observed on the grain boundaries.

1. Introduction

Recently, the microstructures, oxidation resistance and mechanical properties of the austenitic Fe–Al–Mn–C alloys have been studied extensively [1–23]. In Fe–Al–Mn–C alloy system, Al stabilizes the ferritic phase and improves the anti-corrosion behavior, because the formation of a protective Al_2O_3 layer on the surface continuously [1–3]. Mn is added to stabilize the austenitic structure, and enhances mechanical properties at high temperatures [2,4–6]. Furthermore, C is not only an austenite (γ) former but also an important element for promoting precipitating strength of Fe–Al–Mn–C alloy [6,7]. As C content between 0.5 and 1.5 wt.% could lead to some fine κ-phase carbides ($(Fe, Mn)_3AlC_x$) with $L'1_2$ structure precipitated coherently within γ matrix during aging [8,9]. The formation of κ-phase is considered to be a possible strengthening mechanism for Fe–Al–Mn–C alloy system as it raises the yielding strength significantly. It is generally concluded that the Fe–Al–Mn–C alloys have numerous superior features including low density, low magnetism, well-corrosion resistance, high strength, good biocompatibility, etc. [7,10–12]. In addition, an optimal chemical compositions of Fe–Al–Mn–C alloys are in the range of Fe–(4.9–11.0 wt.%)Al–(23.7–35 wt.%)Mn–(0.5–1.5 wt.%)C [2,5,13–15]. Thus, the Fe–Al–Mn–C alloys are suitable for industrial use and in biomedical applications.

However, in order to increases the anti-high temperature corrosion behavior and oxidation resistance as well as strength, some metallic elements Si, Cu, Ti, V, Nb, Mo, W, Cr etc. are added [5,9,16,17]. The Mo addition in Fe–Al–Mn–C alloy can promote the mechanical strength at high temperatures [5]. The addition of Si would enhance the formation of the ferrite phase in the Fe–Al–Mn–C alloy [9]. In addition, it revealed that addition of Si into the Fe–Al–Mn–C alloy improves their high temperature oxidation resistance [18,19]. Among of these metallic elements, Cr was found to be the most effective to improve the high temperature oxidation resistance and environmental embrittlement in the Fe–Al–Mn alloys [17,20,21]. Moreover, Lee et al. [20] also pointed out that increasing the Cr addition would expand both the A12 α-Mn and DO_3 phase-field regions in the Fe–Al–Mn alloy. As stated above, no information concerning the microstructural influences of Cr addition on Fe–Al–Mn–C alloy has been reported. Therefore, the purpose of the present study is an attempt to investigate the phase transformations of the Fe–8.7Al–28.3Mn–1C alloy containing 5.5 wt.% Cr, providing information that is valuable to industrial applications.

* Corresponding author at: School of Dentistry, College of Dental Medicine, Kaohsiung Medical University, Kaohsiung 807, Taiwan. Tel.: +886 73121101x7003; fax: +886 73210637.
** Co-Corresponding author.
E-mail addresses: klou@tmu.edu.tw (K.-L. Ou), chhswa@kmu.edu.tw (C.-H. Wang).

0925-8388/$ – see front matter © 2009 Elsevier B.V. All rights reserved.
doi:10.1016/j.jallcom.2009.08.097

Table 1
Chemical compositions of the present alloy and phase in different condition revealed by an energy-dispersive spectrometer (EDS).

Condition	Alloy and phase	Chemical composition (wt.%)				
		Fe	Al	Mn	C	Cr
Casting	Present alloy	Bal.	8.72	28.31	1.05	5.53
SHT 1300 °C/5 min	γ-Phase(α + B2 + DO_3)-Phase	Bal.Bal.	8.5310.51	28.1627.03	0.830.12	3.826.03
Aging 500 °C/4 h	γ-Phase κ-Phase	Bal.Bal.	8.02 9.14	30.5430.44	0.624.51	4.235.03
Aging600 °C/30 min	$Cr_{23}C_6$	Bal.	6.62	28.35	0.83	42.11
Aging 600 °C/8 h	Cr_7C_3	Bal.	8.52	28.14	8.55	52.14

2. Experimental procedures

The alloy of interest was prepared in an air induction furnace in a protective atmosphere N_2 using AISI 1008 low carbon steel, 99.7% pure electrolytic aluminum, 99.9% pure electrolytic manganese, pure carbon powder, and pure chromium. The alloy was poured into the Ø40 mm × 100 mm investment casting mould preheated at 1160–1180 °C. The chemical compositions of the present alloy were identified by inductively coupled plasma atomic emission spectrometry (ICP-AES), as presented in Table 1. After it was homogenized at 1200 °C for 4 h in a protective argon atmosphere, the ingot was hot-forged to a final thickness of 3.0 mm. The as-forged specimens were heat-treated at temperature from 400 to 1400 °C for various periods in a vacuum furnace, before being then quenched rapidly at room temperature. The surface morphologies of the specimens following treatments were analyzed by optical microscopy (OM) and scanning electron microscopy (SEM, JEOL JSM-6380). The etching solution used was 5–10% nital solution. Elemental distributions were examined using an energy-dispersive X-ray spectrometer (EDS). Quantitative analyses of elemental concentration for Fe, Al, Mn and Cr were conducted using a corrected program on the EDS system. The phase transformation of the specimens after treatments was investigated by means of a scanning transmission electron microscopy (STEM, JEOL-2000FX) at 200 kV. The TEM specimens were prepared using a double twin-jet electropolisher with an electrolyte of 60% ethanol, 30% acetic acid and 10% perchloric acid. The polishing temperature was maintained in the range −15 to 0 °C, and the current density was maintained in the range from 1.5 to 2.5 × 10^4 A/cm^2.

3. Results and discussion

All of the as-forged specimens were underwent solution heat treatment (SHT) process to cause them to have a single austenite structure before their phase transformation was analyzed. As the alloy had underwent SHT in the range 800–1000 °C, its microstructure was essentially a mixture of γ and/or (γ + streak precipitates) regions. These streak precipitates were formed in the matrix and grain boundaries. Moreover, the amounts of these streak precipitates increased with the SHT temperature and time. Fig. 1 displays a bright field (BF) electron micrograph of the [1 1 1] zone of the γ matrix of the alloy that had been heat treated at 900 °C for 30 min, suggesting that these streak precipitates were Cr_7C_3-phase carbide with a hexagonal structure and lattice parameters of a = 1.393 nm and c = 0.452 nm. Therefore, when the alloy underwent SHT at 800–1000 °C, its microstructure became a mixture of the γ + Cr_7C_3-carbide phases. The microstructure of the alloy following SHT at 1050–1200 °C was a single austenite phase with the (1 1 1) habit plane annealing twins.

Increasing the SHT temperature to between 1250 and 1400 °C produced some re-solidificated (RS) regions on the grain boundaries. The sizes of the RS regions increased with the SHT temperature. Fig. 2 presents a BF electron micrograph of the alloy that had been solution-treated at 1300 °C for 5 min, which was taken from the RS region in the [1 1 0] zone, revealing that the RS region was α-phase with BCC structure. Selected area diffraction pattern (SADP) also revealed the DO_3-phase in the α-phase region, and since the $\vec{g} = 2\,0\,0$ reflection intensity was similar to the $\vec{g} = 1\,1\,1$ reflection intensity, the B2 and DO_3-phase were consists in the same $\vec{g} = 2\,0\,0$ reflection spot (not shown). The DO_3-phase and B2-phase lattice parameter were a = 0.565 and 0.282 nm, respectively. No κ-phase carbide was formed on the grain boundaries. Basically, when the temperature was increased to 1400 °C, the microstructure of the alloy was dendritic. Therefore, in the SHT condition, the microstructure in the present alloy is the mixture of the γ + (α + B2 + DO_3)-phases.

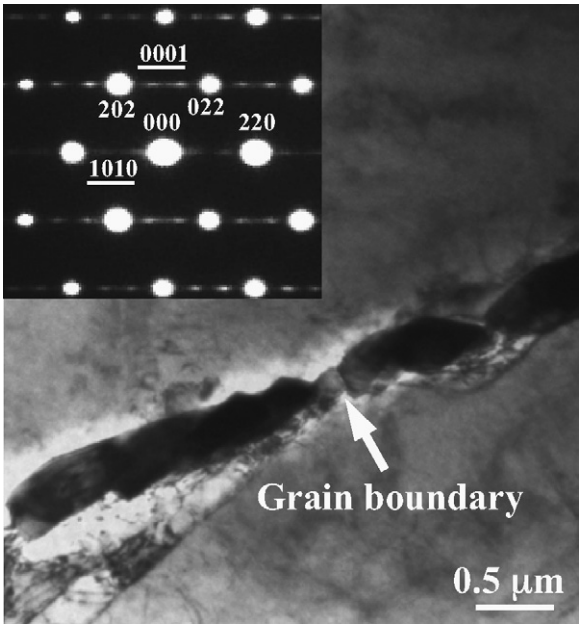

Fig. 1. An electron micrograph of the alloy that had been SHT at 900 °C for 30 min (*hkl* = γ matrix; *hkil* = Cr_7C_3-carbide).

While the as-quenched alloy being aged at 400–500 °C, some κ-phase carbides formed within the γ matrix. The amounts of the κ-phase carbides increased with increasing the aging temperature.

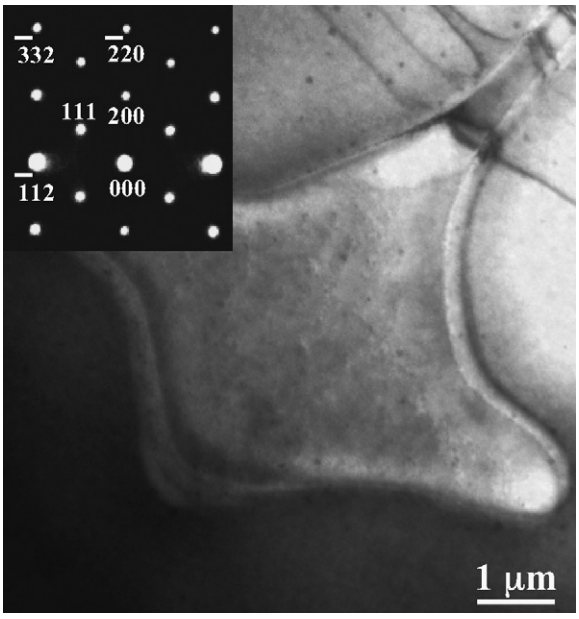

Fig. 2. An electron micrograph of the alloy that had been SHT at 1300 °C for 5 min.

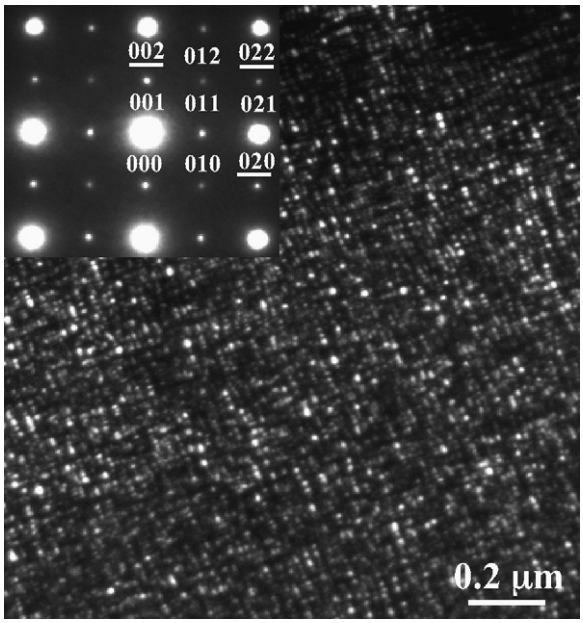

Fig. 3. An electron micrograph of the alloy aged at 450 °C for 8 h (*hkl* = κ-phase; *hkl* = γ matrix).

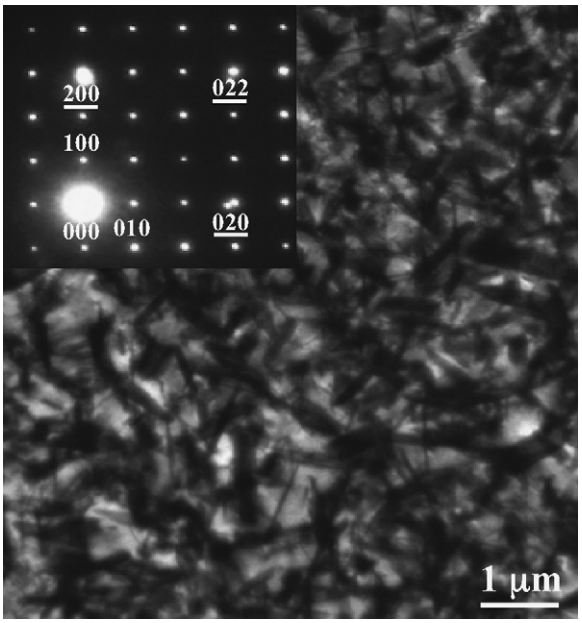

Fig. 5. An electron micrograph of the austenite matrix of the alloy aged at 550 °C for 30 min (*hkl* = $Cr_{23}C_6$-carbide; *hkl* = γ matrix).

Fig. 3 presents a dark field (DF) electron micrograph of the alloy that had been aged at 450 °C for 8 h; it was taken from the γ matrix of the aged alloy in the [1 0 0] zone, revealing that as well as the reflection spots associated with the γ-phase, the SADP also comprises small superlattice spots. Therefore, the tetragonal shape precipitate is κ-phase carbide ($(Fe, Mn)_3AlC_x$) with an ordered $L'1_2$-type structure with the lattice parameter $a = 0.383–0.386$ nm [7,9,22]. The lattice parameter of $(Fe, Mn)_3AlC_x$ κ-phase carbide has been widely reported by other researchers [8,9,23]. The microstructure of the alloy that had been aged at 400–500 °C was a mixture of (γ + κ).

When the aging temperature was increased to 550–650 °C for a short period approximately 30 min, some small black particles were precipitated in the γ matrix and grain boundaries as shown in Fig. 4. Fig. 5 depicts a BF electron micrograph of γ matrix of the [1 0 0] zone of the alloy that was aged at 550 °C for 30 min, revealing that in addition to the reflection spots of the γ-phase, the SADP consist of some extra superlattice spots. The black needle precipitate had a simple cubic structure with lattice parameter $a = 1.054$ nm. These needle precipitates were chromium carbide $Cr_{23}C_6$. The SADP also demonstrated that the orientation relationship between the matrix and the $Cr_{23}C_6$-phase carbide was cubic to cubic.

Furthermore, some DO_3 regions were observed on the grain boundaries. However, as the aging time increased, some coarse particulate precipitates were found in the matrix and grain boundaries. Fig. 6 displays a BF electron micrograph of the γ matrix of the [1 1 0] zone of the alloy that was aged at 550 °C for 8 h, indicating that the coarse particulate precipitates were chromium carbide (Cr_7C_3) The SADP also demonstrates that the orientation relationship between the matrix and the chromium

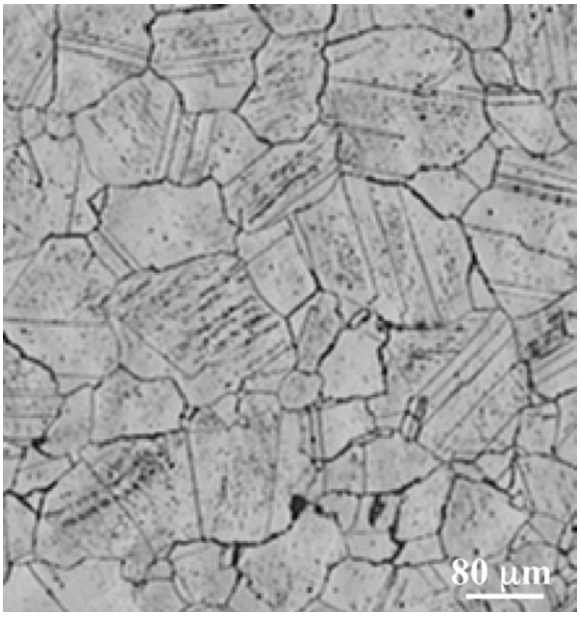

Fig. 4. An optical micrograph of the alloy aged at 550 °C for 30 min.

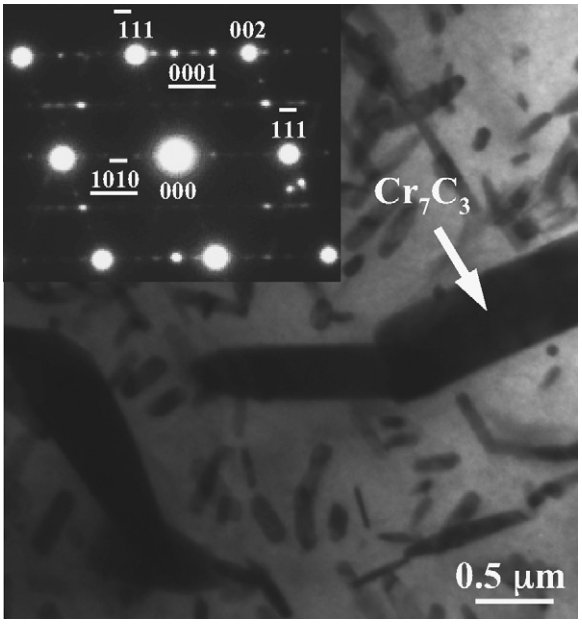

Fig. 6. An electron micrograph of the alloy aged at 550 °C for 8 h (*hkl* = γ matrix; *hkil* = Cr_7C_3-carbide).

carbide (Cr_7C_3) is $[1\bar{1}0]_\gamma//[01\bar{1}0]_{Cr_7C_3}$ and $(111)_\gamma//(0001)_{Cr_7C_3}$. Therefore, when the as-quenched alloy was aged at 550–650 °C, a $\gamma \rightarrow (\gamma + Cr_{23}C_6) \rightarrow (\gamma + Cr_{23}C_6 + Cr_7C_3)$ phase transition occurred within the γ matrix. A $\gamma \rightarrow (DO_3 + Cr_{23}C_6) \rightarrow (DO_3 + Cr_{23}C_6 + Cr_7C_3)$ phase transition was observed on the grain boundaries. When the aged temperature was increased to 700–800 °C, the amounts of Cr_7C_3 phase increased with the aging temperature. No $Cr_{23}C_6$ or DO_3 phase was found in the matrix or grain boundaries. Accordingly, when the as-quenched alloy was aged at 700–800 °C, a $\gamma \rightarrow (\gamma + Cr_7C_3)$ phase transition was observed within the γ matrix. Moreover, a $\gamma \rightarrow (DO_3 + Cr_7C_3)$ phase transition was found on the grain boundaries.

On the basis of the above observations, when the alloy underwent SHT at 1300 °C, some RS ($\alpha + B2 + DO_3$) regions were formed in the matrix and grain boundaries. Accordingly, the melting point of the Al element was lower than that of others alloy elements in the alloy. Hence, the Al element diffused and/or segregated at this high temperature. The liquidus temperature of the Fe–8.7Al–28.3Mn–1C–5.5Cr alloy was around 1300 °C. Accordingly, SEM-EDS was employed to identify the RS regions in the matrix and grain boundaries. Table 1 presents quantitatively the chemical compositions of the γ matrix and RS region of the alloy that had underwent SHT at 1300 °C. Table 1 clearly demonstrates that the Al and Cr contents in the RS region exceeded those in the γ matrix. Accordingly, the RS regions were formed on the grain boundaries because of the Al diffused and/or segregated of the alloy had underwent SHT at 1300 °C. Moreover, the Cr content in the RS region exceeded that in the γ matrix, suggesting that the Al and Cr contents influenced the liquidus temperatures in the alloy.

Table 1 presents quantitatively the chemical compositions of the γ matrix and κ-phase carbide of the alloy that had been aged at 500 °C for 4 h; the concentration of carbon in the κ-phase carbide substantially exceeds that in the γ matrix. Therefore, the κ-phase carbides are expected to have been formed in the γ matrix and grain boundaries. Furthermore, when the aging temperature was increased to 550–650 °C, the chromium carbides ($Cr_{23}C_6$ and Cr_7C_3) were observed in the γ matrix and grain boundaries. Table 1 also presents quantitative chemical compositions of $Cr_{23}C_6$ phase in the alloy that had been aged at 600 °C for 30 min, and Cr_7C_3 phase in the alloy that had been aged at 600 °C for 8 h. The concentration of carbon in the Cr_7C_3 significantly is much greater than that in the $Cr_{23}C_6$, revealing that the carbon content in the γ matrix declined with the aging temperature and time increased. Thus, no κ-phase carbides were formed within the γ matrix and grain boundaries, as the alloy aged at the temperature in the range of 550–650 °C.

4. Conclusions

The microstructure of the as-forged specimen was austenite with some stress-induced twins. Moreover, when the alloy underwent SHT between 800 and 1000 °C, the microstructure thus formed was a mixture of the ($\gamma \pm Cr_7C_3$) phases. Increasing the SHT temperature to 1050–1200 °C yielded a single austenite phase with (1 1 1) annealing twins. When the alloy underwent SHT at 1250–1400 °C, some RS regions formed in the matrix and grain boundaries. The RS region was a mixture of $\gamma + (\alpha + B2 + DO_3)$ phases. When the alloy was aged at 400–500 °C, some $(Fe, Mn)_3AlC_x$ κ-phase carbides were formed in the matrix and grain boundaries. Increasing the aging temperature to 550–650 °C, caused a $\gamma \rightarrow (\gamma + Cr_{23}C_6) \rightarrow (\gamma + Cr_{23}C_6 + Cr_7C_3)$ phase transition in the matrix. Furthermore, a $\gamma \rightarrow (DO_3 + Cr_{23}C_6) \rightarrow (DO_3 + Cr_{23}C_6 + Cr_7C_3)$ phase transition was observed on the grain boundaries. Moreover, when the alloy was aged at 700–800 °C, a $\gamma \rightarrow (\gamma + Cr_7C_3)$ phase transition was occurred in the matrix, and a $\gamma \rightarrow (DO_3 + Cr_7C_3)$ phase transition was observed on the grain boundaries.

Acknowledgements

The work was financially supported by the National Science Council of the Republic of China under Contract No. NSC96-2314-B-038-32 and supported partly by Taipei Medical University Hospital under contract 98TMU-TMUH-03-01 and Biomate Medical Devices Technology Co. Ltd., Taiwan.

References

[1] C.J. Wang, J.W. Lee, T.H. Twu, Surf. Coat. Technol. 163–164 (2003) 37.
[2] C.J. Wang, Y.C. Chang, Mater. Chem. Phys. 76 (2002) 151.
[3] S.C. Chan, Y.H. Hsian, J. Mater. Sci. 24 (1989) 1117.
[4] J.D. Betancur-Ríos, J.A. Tabares, G.A. Pérez Alcázar, V.F. Rodríguez, Hyperfine Interact. 175 (2007) 63.
[5] J.D. Betancur-Rios, K. Nomura, C.J. Wang, G.A. Pérez Alcazar, J.A. Tabares, Hyperfine Interact. 187 (2008) 43.
[6] M.C. Li, H. Chang, P.W. Kao, D. Gan, Mater. Chem. Phys. 59 (1999) 96.
[7] C.Y. Chao, C.H. Liu, Mater. Trans. 43 (10) (2002) 2635.
[8] C.S. Wang, C.N. Hwang, C.G. Chao, T.F. Liu, Scripta Metall. 57 (2007) 809.
[9] J.W. Lee, T.F. Liu, Mater. Chem. Phys. 69 (2001) 192.
[10] R. Umino, X.J. Liu, Y. Sutou, C.P. Wang, I. Ohnuma, R. Kainuma, K. Ishida, J. Phase Equilib. Diff. 27 (1) (2006) 54.
[11] S.L. Chen, M.H. Lin, C.C. Chen, K.L. Ou, J. Alloys Compd. 456 (2008) 413.
[12] P.R. Rao, V.V. Kutumbarao, Int. Mater. Rev. 34 (2) (1989) 69.
[13] C.W. Su, J.W. Lee, C.S. Wang, C.G. Chao, T.F. Liu, Surf. Coat. Technol. 202 (2008) 1847.
[14] J.W. Lee, J.G. Duh, J.H. Wang, Surf. Coat. Technol. 168 (2003) 223.
[15] P. Pérez, F.J. Pérez, C. Gómez, P. Adeva, Corros. Sci. 44 (2002) 113.
[16] B. Bhattacharya, A.S. Sharma, S.S. Hazra, R.K. Ray, Metall. Trans. A 40A (2009) 1190.
[17] J.G. Duh, S.C. Lin, J. Mater. Sci. 28 (1993) 5975.
[18] J.G. Duh, L.W. Lee, C.J. Wang, J. Mater. Sci. 23 (1998) 2649.
[19] V. De Freitas Cunha Lins, M.A. Freitas, E.M. De Paula e Silva, Corros. Sci. 46 (2004) 1895.
[20] J.W. Lee, C.C. Wu, T.F. Liu, Scripta Metall. 50 (2004) 1389.
[21] J.W. Lee, J.G. Duh, S.Y. Tsai, Surf. Coat. Technol. 153 (2002) 59.
[22] C.Y. Chao, C.N. Hwang, T.F. Liu, Scripta Metall. 34 (1) (1996) 75.
[23] K. Sato, K. Tagawa, Y. Inoue, Metall. Trans. A 21A (1990) 5.